

Highly stable porous-carbon-coated Ni catalysts for the reductive amination of levulinic acid via an unconventional pathway

Guang Gao, Peng Sun, Yunqin Li, Fang Wang, Zelun Zhao, Yong Qin, and Fuwei Li

ACS Catal., **Just Accepted Manuscript** • Publication Date (Web): 19 Jun 2017

Downloaded from <http://pubs.acs.org> on June 19, 2017

Just Accepted

“Just Accepted” manuscripts have been peer-reviewed and accepted for publication. They are posted online prior to technical editing, formatting for publication and author proofing. The American Chemical Society provides “Just Accepted” as a free service to the research community to expedite the dissemination of scientific material as soon as possible after acceptance. “Just Accepted” manuscripts appear in full in PDF format accompanied by an HTML abstract. “Just Accepted” manuscripts have been fully peer reviewed, but should not be considered the official version of record. They are accessible to all readers and citable by the Digital Object Identifier (DOI®). “Just Accepted” is an optional service offered to authors. Therefore, the “Just Accepted” Web site may not include all articles that will be published in the journal. After a manuscript is technically edited and formatted, it will be removed from the “Just Accepted” Web site and published as an ASAP article. Note that technical editing may introduce minor changes to the manuscript text and/or graphics which could affect content, and all legal disclaimers and ethical guidelines that apply to the journal pertain. ACS cannot be held responsible for errors or consequences arising from the use of information contained in these “Just Accepted” manuscripts.



Highly stable porous-carbon-coated Ni catalysts for the reductive amination of levulinic acid via an unconventional pathway

Guang Gao,^{†,§} Peng Sun,^{†,§} Yunqin Li,^{‡,§} Fang Wang,[†] Zelun Zhao,[†] Yong Qin,^{‡,*} and Fuwei Li^{†,*}

[†]State Key Laboratory for Oxo Synthesis and Selective Oxidation, Suzhou Research Institute of LICP, Lanzhou Institute of Chemical Physics (LICP), Chinese Academy of Sciences, Lanzhou 730000, P. R. China.

[‡]State Key Laboratory of Coal Conversion, Institute of Coal Chemistry, Chinese Academy of Sciences, Taiyuan 030001, P. R. China.

ABSTRACT: The catalytic conversions of biomass and its derivatives into fuels and chemicals require active and stable catalysts. Non-noble-metal catalysts typically suffer from deactivation due to the leaching and sintering of the metal species in liquid-phase reactions. In this work, we report a facile synthesis of porous-carbon-coated Ni catalysts supported on carbon nanotubes (CNF_x@Ni@CNTs) by atomic layer deposition for the reductive amination of levulinic acid (LA) with amines to pyrrolidones. Under the protection of porous carbon with a moderate thickness, the optimized CNF₃₀@Ni@CNTs catalyst showed a 99% yield of pyrrolidones and recyclability of up to 20 runs without the leaching and sintering of Ni nanoparticles. Based on verification experiments and density functional theory calculations, we determined that our Ni-catalyzed reductive amination of LA with amines underwent an unconventional pathway via amides as the first intermediate, followed by tandem cyclization, intramolecular dehydration and hydrogenation to the desired pyrrolidones. This pathway was completely different from the reported imine-intermediated route in Pt-catalyzed systems. This work provides insights into the design of active and stable heterogeneous catalysts for liquid-phase reactions as well as into switching reaction pathways to realize the replacement of noble metals for the transformation of bio-based multifunctional substrates.

KEYWORDS: *catalyst stability, atomic layer deposition, reaction pathway, biomass conversion, levulinic acid*

1. INTRODUCTION

Over the past decade, the energy crisis has driven numerous studies on the conversion of biomass into fuels and valuable chemicals.¹⁻¹⁰ Unlike petroleum-based raw materials, biomass feedstocks are highly functionalized and thermally unstable, thus making them very difficult to be refined in the gas phase. Consequently, catalytic upgrading is typically performed in liquid-phase reactions.¹¹⁻¹⁷ In liquid media, heterogeneous metal catalysts typically suffer from irreversible deactivation caused by active metal species leaching into solution.^{18,19} This deactivation greatly impedes the utilization of a catalyst in industrial processes, as the replacement of the deactivated catalyst requires shutdown and disposal of solid waste.²⁰ Therefore, the catalyst stability is crucial to the economic and environmental sustainability of a catalytic process.

An effective strategy to prevent active metal species from leaching and sintering is encapsulating metal catalysts within a protective “overcoat”, such as a two-dimensional material,^{21,22} metal oxide^{20,23} or micro-/mesoporous zeolite.²⁴⁻³¹ The overcoats should be sufficiently porous to allow the free access of reactants and products to metal surfaces.²⁹ Additionally, the overcoat thickness is critical to the catalytic performance. A thick coating has a negative impact on mass transfer, while too thin of an overcoat may allow metal leaching. Accordingly, the precise control of the coating thickness on the atomic scale is intensively desired. Atomic layer deposition (ALD) is a useful technique that can precisely tailor the thickness of a thin film as well as control the size of nanoparticles/nanoclusters in the design and preparation of a catalyst.³²⁻⁴²

Levulinic acid (LA) is a sustainable platform molecule from biomass.⁴³⁻⁴⁶ LA contains one carbonyl and one carboxyl group in its structure, which can react with amines to provide imines and amides, respectively. Recently, the reductive amination of LA with amines to pyrrolidones, important compounds as surfactants, solvents, and intermediates for pharmaceuticals, has been studied using supported metal catalysts.⁴⁷⁻⁵⁶ In these works, imines were recognized as the first intermediates formed over noble-metal catalysts.^{49,51,52,56} Most literature has focused on improving the catalytic activity and selectivity of this transformation. However, these reports have only occasionally discussed the stability issues of the metal catalysts, especially involving non-noble metals.

Herein, we report a facile ALD approach for the synthesis of porous-carbon-coated Ni nanoparticles (NPs) supported on carbon nanotubes (CNTs) (CNF_x@Ni@CNTs) for the reductive amination of LA with amines to pyrrolidones. We elaborately tailored the thickness of the porous carbon nanofilms by simply controlling the number of ALD cycles. The optimized CNF₃₀@Ni@CNTs catalyst was very stable in the liquid phase and could be reused up to 20 runs without the loss of activity, while the conventional bare Ni catalyst showed poor stability due to severe Ni leaching. Finally, we proposed an alternative Ni-catalyzed reaction pathway via amide intermediates, which was verified by the combination of confirmatory experiments and density functional theory (DFT) calculations.

2. RESULTS AND DISCUSSION

2.1. Preparation of CNF_x@Ni@CNTs Catalysts and their Application in the Reductive Amination of LA

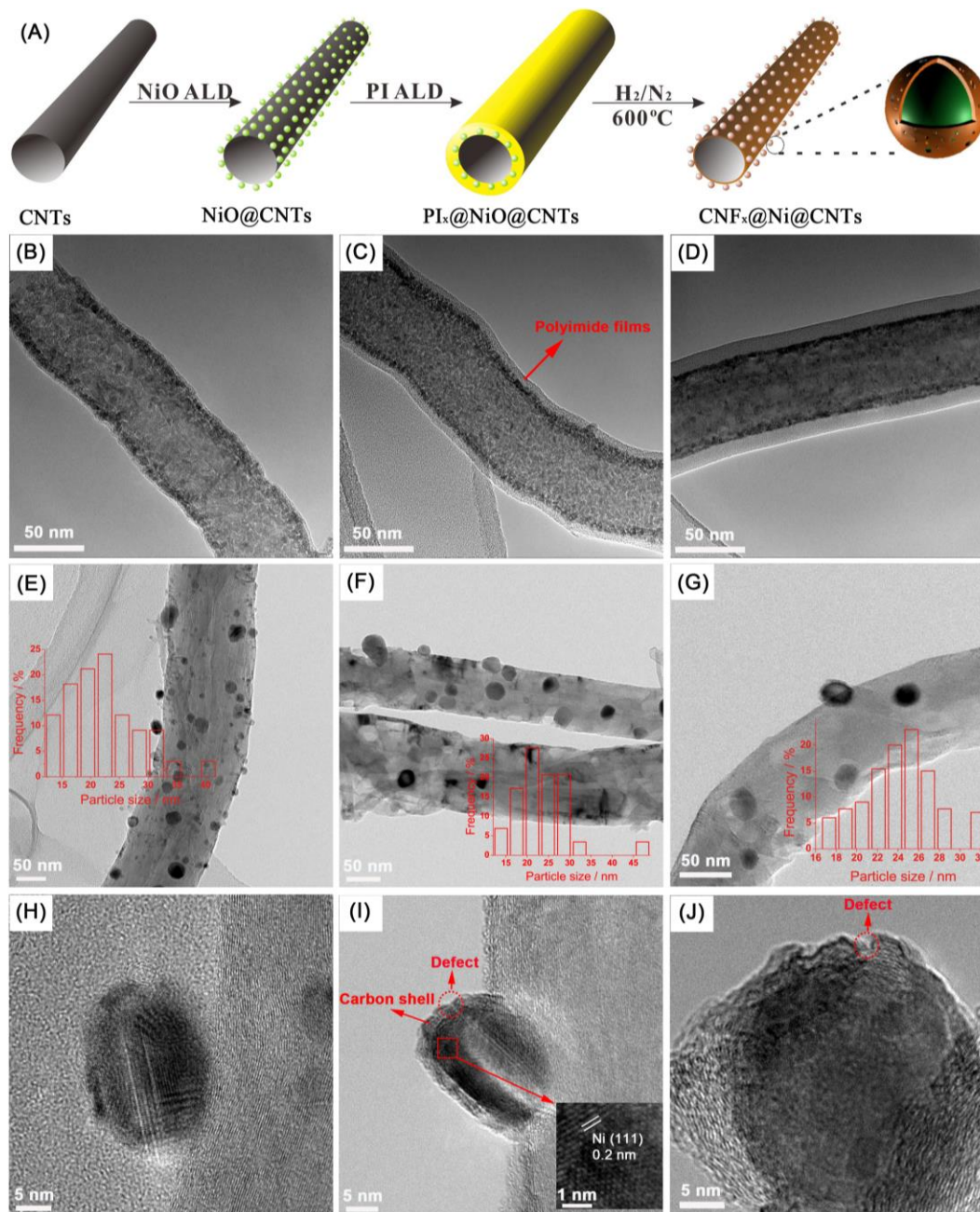


Figure 1. (A) Illustration of the catalyst preparation; TEM images of (B-D) $\text{PI}_x\text{@NiO@CNTs}$, (E, H) $\text{CNF}_{10}\text{@Ni@CNTs}$, (F, I) $\text{CNF}_{30}\text{@Ni@CNTs}$ and (G, J) $\text{CNF}_{80}\text{@Ni@CNTs}$.

Figure 1A illustrates the preparation procedure for the $\text{CNF}_x\text{@Ni@CNTs}$ catalysts. NiO NPs and polyimide (PI) films were sequentially deposited on CNTs by ALD to give $\text{PI}_x\text{@NiO@CNTs}$, where x represents the number of ALD cycles of the deposited PI films. The obtained samples were then treated with a 10% H_2/N_2 mixture at 600 °C. During the treatment, the PI films were pyrolyzed to carbon nanofilms, while the NiO NPs were simultaneously reduced to metallic Ni NPs, eventually providing the $\text{CNF}_x\text{@Ni@CNTs}$ catalysts. Inductively coupled plasma-atomic emission spectroscopy (ICP-AES) confirmed the Ni content in each sample as 10 wt %. Transmission electron microscopy (TEM) images of as-prepared $\text{PI}_x\text{@NiO@CNTs}$ showed that the CNTs were clearly coated with uniform PI films. The thicknesses of PI films were approximately 3.3, 5.5 and 22.5 nm after 10, 30 and 80 ALD cycles, respectively (Figure 1B-D). After calcination, all the $\text{CNF}_x\text{@Ni@CNTs}$ catalysts showed uniform Ni NPs with

average diameters of 22-24 nm on the surface of CNTs (Figure 1E-G). After ten cycles of the PI films, the obtained carbon nanofilms were very thin, beyond our observational detection limits (Figure 1H). When the number of ALD cycles was increased to 30 and 80, the Ni NPs were coated by few-layer carbon shells with thicknesses of 2.0-2.4 (Figure 1I) and 3.0-6.0 nm (Figure 1J), respectively. Upon pyrolyzation, the PI layer largely shrunk, thus creating numerous micropores and/or mesopores in the carbon shells.^{57,58} Notably, the carbon shells were not perfectly closed, with lots of defects such as small channels, as demonstrated in Figure 1I and 1J, allowing the underlying Ni NPs to be accessible to substrates. The inset image in Figure 1I demonstrates a lattice d -spacing of 0.2 nm, well consistent with the (111) planes of metallic Ni.²¹

N_2 adsorption/desorption measurements were then performed to investigate the porous structures of the carbon-coated Ni@CNTs catalysts.

Table 1. Reductive amination of LA with benzyl (Bn) amine over various catalysts^a

| Entry | Catalyst | Yields / % | | |
|-------|------------------------------------|-----------------------|-----------------------|----|
| | | M3 | BMP | M4 |
| 1 | Ni@CNTs | 1 (34 ^b) | 99 (65 ^b) | - |
| 2 | CNF ₁₀ @Ni@CNTs | 1 (32 ^b) | 99 (68 ^b) | - |
| 3 | CNF ₂₀ @Ni@CNTs | 1 (31 ^b) | 99 (69 ^b) | - |
| 4 | CNF ₃₀ @Ni@CNTs | 1 (30 ^b) | 99 (69 ^b) | - |
| 5 | CNF ₅₀ @Ni@CNTs | 26 (72 ^b) | 72 (28 ^b) | - |
| 6 | CNF ₈₀ @Ni@CNTs | 27 (73 ^b) | 70 (26 ^b) | - |
| 7 | Ni/CNTs | 8 | 90 | - |
| 8 | Ni/C | 1 | 99 | - |
| 9 | Ni/TiO ₂ ^c | 33 | 34 | 17 |
| 10 | Ni/NbOPO ₄ ^c | 31 | 42 | 22 |
| 11 | Ni/HZSM-5 ^c | 21 | 21 | 36 |
| 12 | Ni/SAPO-34 ^c | 25 | 32 | 26 |
| 13 | Blank ^c | 32 | - | 29 |

^aReaction conditions: LA (10 mmol), BA (10 mmol), catalyst (0.03 g, 10 wt % Ni), γ -valerolactone as a solvent (4 mL), 3.0 MPa H₂, 130 °C, and 6 h. ^bReaction time of 4 h. ^cThe other products are mainly *N*-benzyl-4-oxopentanamide (**M1**) and 1-benzyl-5-hydroxy-5-methylpyrrolidin-2-one (**M2**), and their yields are listed in Table S1. **M3**: 1-benzyl-5-methylenepyrrolidin-2-one, **BMP**: 1-benzyl-5-methylpyrrolidin-2-one, **M4**: 1-benzyl-4-(1-benzyl-2-methyl-5-oxopyrrolidin-2-yl)-5-methyl-1*H*-pyrrol-2(5*H*)-one. Yields of **M3**, **M4** and **BMP** were determined by GC analysis with 1,4-dioxane as an internal standard.

As presented in Figure S1A, the isotherm curves of the Ni@CNTs and CNF₃₀@Ni@CNTs samples displayed typical H3-type hysteresis loops, indicating the existence of slit mesopores, in agreement with the narrow pore size distributions at approximately 4 nm (Figure S1B). Moreover, we found an obvious increase in the pore volume between 2-3 nm for the CNF₃₀@Ni@CNTs sample, implying the generation of more mesopores during the carbonization of PI.⁵⁹ The Brunauer-Emmett-Teller (BET) surface area of CNF₃₀@Ni@CNTs (102 m² g⁻¹) was higher than that of Ni@CNTs (88 m² g⁻¹) (entries 1 and 2, Table S1), further proving the existence of abundant pores surrounding the Ni NPs. Such porous shells guarantee that the underlying metal surfaces will be easily accessed by reactants.

The prepared CNF_x@Ni@CNTs catalysts were applied to the reductive amination of LA with benzyl amine (BA) to 1-benzyl-5-methylpyrrolidin-2-one (**BMP**). As listed in Table 1 (data in parentheses), after 4 h of reaction, the **BMP** yields over the CNF_x@Ni@CNTs catalysts with small number of ALD cycles ($x = 10, 20, \text{ and } 30$) were nearly identical (68-69%, entries 2-4). As a reference, uncoated Ni@CNTs showed a slightly lower yield (65%, entry 1), indicating that the thin overcoats did not block the exposure of the underlying active metal and mass transport. However, under the same conditions, only 28% and 26% yields of **BMP** were obtained over CNF₅₀@Ni@CNTs and CNF₈₀@Ni@CNTs (entries 5 and 6), respectively, suggesting that the thick shells greatly impede mass transfer and thus slow the reaction rates. Importantly, we

also detected an important unsaturated product, 1-benzyl-5-methylenepyrrolidin-2-one (**M3**), with a yield of 30-73% (entries 1-6) in all 4 h reaction systems. As **M3** can be easily converted to **BMP** via C=C hydrogenation, we believe that **M3** is an essential intermediate to give the final **BMP**.

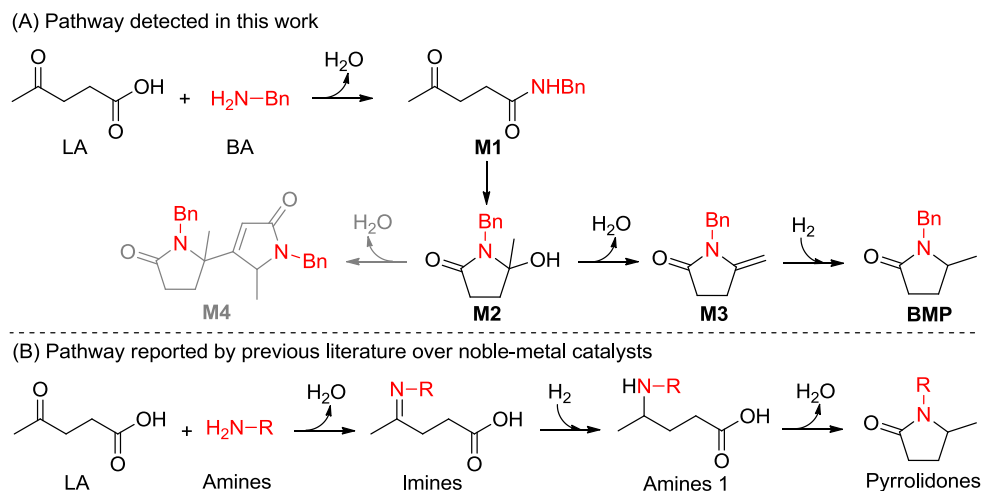
We then prolonged the reaction time to 6 h, and as expected, the amount of **M3** decreased to some extent for all the tested catalysts. Specifically, we obtained nearly complete reactions, with **BMP** yields of 99%, over CNF_x@Ni@CNTs ($x = 0, 10, 20, \text{ and } 30$) (entries 1-4). However, for the CNF_x@Ni@CNTs ($x = 50 \text{ and } 80$) catalysts with thick shells, the **BMP** yields only enhanced to 70-72%, still retaining 26-27% **M3** (entries 5 and 6), proving again the importance of a moderate carbon thickness. We also calculated the turnover number (TON) of the CNF₃₀@Ni@CNTs catalyst. As shown in Table S2, we obtained a high TON of up to 1343 by decreasing the catalyst loading and prolonging the reaction time, which is slightly lower than the TON (1475) of the referenced Pt/C catalyst under the same conditions.

To gain more insight into the effect of the support, we prepared reference catalysts with the Ni catalyst loaded on various supports by an incipient wetness impregnation method, referred to as Ni/supports. As shown in Table 1 (entries 7 and 8), Ni/CNTs and Ni/C (activated carbon) exhibited comparative **BMP** yields as CNF_x@Ni@CNTs ($x = 0, 10, 20, \text{ and } 30$). In contrast, acidic supports, including TiO₂, NbOPO₄, HZSM-5 and SAPO-34 (entries 9-12), had negative influences on the **BMP** yield (only 21-42%), with certain amounts of unreacted precursors (*N*-benzyl-4-oxopentanamide (**M1**), 1-benzyl-5-hydroxy-5-methylpyrrolidin-2-one (**M2**) and **M3**) observed. Additionally, we detected a by-product, 1-benzyl-4-(1-benzyl-2-methyl-5-oxopyrrolidin-2-yl)-5-methyl-1*H*-pyrrol-2(5*H*)-one (**M4**), with a considerable yield varying from 17 to 36%. The above results suggest these acidic supports not only slow the tandem transformation of **M1**, **M2** and **M3** to **BMP** but also favor the formation of the by-products.

The relative acidity of each support was then determined by NH₃ temperature-programmed desorption (NH₃-TPD, Figure S2), and the results are listed in Table S1. The order of acidity was as follows: TiO₂<NbOPO₄<HZSM-5<SAPO-34. After correlating the **BMP** yield with the acidity, a straight-forward linear relationship was not found, as the surface area and Ni particle diameter may also affect the catalytic performance (see detailed discussion in the Supporting Information).

A blank reaction was also performed, showing no detection of **BMP** without a catalyst (entry 13, Table 1). Instead, a considerable amount of **M3** (32%) and **M4** (29%) were found, accompanied with some amounts of **M1** and **M2**, which indicates that the hydrogenation of **M3** to **BMP** was a catalyzed step, while the formations of **M1**, **M2**, **M3** and **M4** were non-catalyzed steps. The Ni catalysts efficiently hydrogenated the C=C bond in **M3**, thus pushing the reaction to **BMP**. Correspondingly, such catalytic hydrogenation inhibited the generation of by-product **M4**.

To examine the real reusability of the Ni catalysts, a reaction time of 4 h was chosen to obtain a moderate **BMP** yield. As shown in Figure 2 (black bar), the CNF₃₀@Ni@CNTs catalyst displayed good stability and was recycled for 20 runs without apparent activity loss. ICP-AES analysis of the filtrate confirmed that the Ni content in the solution was below the detection limit (Table S3). Additionally, the average Ni NPs size in the spent CNF₃₀@Ni@CNTs catalyst (Figure S5) was similar to that of the fresh catalyst (Figure 1F). In contrast, the uncoated Ni@CNTs catalyst prepared by ALD could only be



Scheme 1. Reaction pathways for the reductive amination of LA with amines (A) detected in this work using BA as an example and (B) reported by previous literature.

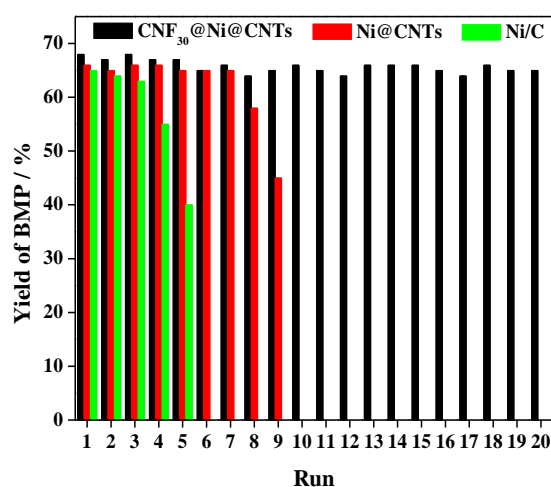


Figure 2. Catalyst reuse study for the reductive amination of LA with BA over CNF₃₀@Ni@CNTs (black), Ni@CNTs (red) and Ni/C (green). Reaction conditions: LA (10 mmol), BA (10 mmol), catalyst (0.03 g, 10 wt % Ni), γ -valerolactone as a solvent (4 mL), 3.0 MPa H₂, 130 °C, and 4 h.

reused seven times. Deactivation of the uncoated Ni@CNTs occurred at the eighth run (red bar) due to Ni leaching, as evidenced from TEM (Figure S6) and ICP-AES (Table S3). The Ni/C catalyst displayed even worse reusability. The **BMP** yield declined significantly at the fourth and fifth runs (green bar). TEM images of the fresh and spent Ni/C catalysts (Figure S7) indicated most of Ni particles were detached after five runs. ICP-AES analysis of the filtrate showed that the Ni content in solution was 7.9 wt % of the original Ni content (Table S3), further suggesting the severe leaching of the Ni NPs. We then performed a hot filtration test to verify the heterogeneity of our reaction. After a 3 h reaction, the Ni/C catalyst was filtered off, and the reaction was re-run for an additional 3 h. Figure S8 depicts that no further formation of **BMP** was detected after removal of Ni/C, demonstrating that our reaction was catalyzed by Ni/C rather than leached Ni NPs in the solution. From the above analyses, we conclude that the outer porous carbon nanofilms effectively protected the underlying Ni NPs against leaching and sintering in the liquid-phase reaction, thus ensuring extraordinary stability of the CNF₃₀@Ni@CNTs catalyst.

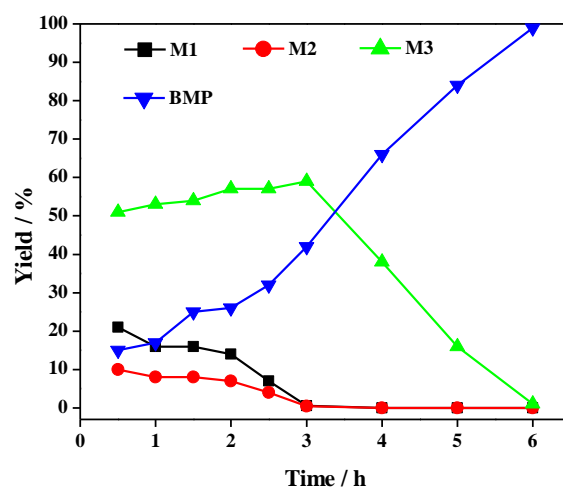


Figure 3. Time-course plots of the reductive amination of LA with BA over the Ni/C catalyst. Reaction conditions: LA (10 mmol), BA (10 mmol), Ni/C catalyst (0.03 g, 10 wt % Ni), γ -valerolactone as a solvent (4 mL), 3.0 MPa H₂, and 130 °C. **M1**: *N*-benzyl-4-oxopentanamide, **M2**: 1-benzyl-5-hydroxy-5-methylpyrrolidin-2-one, **M3**: 1-benzyl-5-methylenepyrrolidin-2-one, **BMP**: 1-benzyl-5-methylpyrrolidin-2-one.

2.2. Verification of the Reaction Pathway Catalyzed by the Ni Catalyst.

To explore the reaction route, we used Ni/C as a model catalyst to analyze the reaction intermediates in our Ni-catalyzed reductive amination of LA with BA. Importantly, the intermediates in our system are quite different from those in noble-metal-catalyzed reactions, suggesting a completely different reaction pathway. Time-course product distributions provided detailed information for the reaction route, as shown in Figure 3. During the reaction, four compounds were isolated and identified by nuclear magnetic resonance (NMR) spectroscopy, infrared spectroscopy (IR) and high-resolution mass spectrometry (HRMS) (see Supporting Information), i.e., **M1**, **M2**, **M3** and **BMP**. The identities of **M1**, **M2** and **M3** as reaction intermediates were preliminarily deduced from their structures (Scheme 1A). As shown in Figure 3, **M1** and **M2** gradually disappeared within 3 h, while the **M3** slightly grew over the first 3 h and then dropped with prolonged time. During the entire period, the **BMP** yield steadily increased up to 99%

Table 2. Rates of LA, M1, M2, M3 transformations at 0.5 h of reaction

| Elementary reaction step | Rate ^a / $\mu\text{mol g}_{\text{cata}}^{-1} \text{s}^{-1}$ | Rate ^b / $\mu\text{mol g}_{\text{cata}}^{-1} \text{s}^{-1}$ |
|--------------------------|--|--|
| LA→M1 | 1852 | 463 |
| M1→M2 | 1463 | 375 |
| M2→M3 | 1317 | 234 |
| M3→BMP | 606 | 161 |
| M2→M4 | - | 96 |

^aEvaluated from Figure 3. ^bEvaluated from Figure S9. Detailed rate calculations are included in the Supporting Information.

after 6 h. This trend clearly indicated that **BMP** was formed via a tandem route through **M1**, **M2** and **M3**. Note that LA and BA were not detected after 0.5 h, implying a fast and complete conversion.

Under solvent-free conditions (Figure S9), another product, **M4**, was detected as a competitive by-product for **BMP**. NMR, IR and HRMS analyses (see the Supporting Information) confirmed the molecular structure of **M4**. 1-Allyl-5-hydroxy-5-methylpyrrolidin-2-one (**R1**) has been reported to undergo intermolecular dehydration to 1-allyl-4-(1-allyl-2-methyl-5-oxopyrrolidin-2-yl)-5-methyl-1H-pyrrol-2(5H)-one (**R2**) (Scheme S1).⁶⁰ Our NMR, IR and HRMS analyses showed that **M2** and **M4** had similar structures to **R1** and **R2**, respectively. Therefore, we propose that **M4** is formed via the intermolecular dehydration of **M2**, as presented in Scheme 1A.

We next calculated the reaction rates of LA→**M1**, **M1**→**M2**, **M2**→**M3**, **M3**→**BMP**, and **M2**→**M4** over Ni/C based on the data at 0.5 h from Figures 3 and S9 (detailed calculation method provided in the Supporting Information), as summarized in Table 2. The transformation of LA to **M1** was faster than the subsequent four reaction steps. The hydrogenation rate of **M3** to **BMP** was the slowest, suggesting this step as rate limiting. Importantly, the rate of each step using γ -valerolactone as the solvent was much higher than that without a solvent, indicating that γ -valerolactone not only prevented the formation of undesired **M4** but also accelerated the generation of the targeted **BMP**. Moreover, various solvents were studied, and we screened the bio-derived γ -valerolactone as the best solvent to produce **BMP** (Table S4, see further discussion in the Supporting Information).

Notably, the first intermediate (**M1**) in the Ni-catalyzed system is an amide, which is quite different from the reported imine as the first intermediate in the Pt-catalyzed reaction. Considering the C=N hydrogenation step as the key to between the imine/amide, we compared Pt/C and Ni/C in the reduction of *N*-benzylpentan-2-imine (**1a**), which is structurally similar to LA. Since the **1a** hydrogenation rate over Pt/C was too fast to track record, the Pt/C loading was decreased to one fifth that of Ni/C. As shown in Figure 4, the TON of Pt/C was much higher than that of Ni/C, implying Pt/C possesses a higher C=N bond hydrogenation activity to produce *N*-benzylpentan-2-amine (**1b**).

To deeply understand the difference in the C=N hydrogenation activity between Ni/C and Pt/C, we calculated the C=N bond distances, adsorption energies of **1a** and charge states of the N atoms on Ni(111) and Pt(111) surfaces by DFT calculations with the adsorption models described in Figure 5.

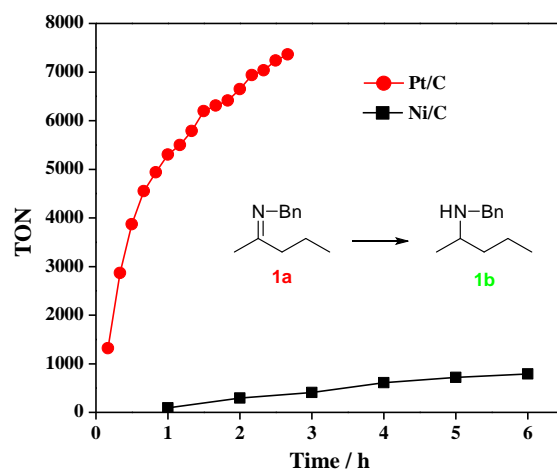


Figure 4. TONs for the hydrogenation of **1a** over the Pt/C and Ni/C catalysts. The TON is calculated as the moles of **1b** / moles of Ni or Pt. Reaction conditions: **1a** (10 mmol), Pt/C (0.002 g, 5 wt % Pt) or Ni/C (0.01 g, 10 wt % Ni), THF as a solvent (4.0 mL), 3.0 MPa H₂, and 130 °C.

Table 3. Reductive amination of pentan-2-one with BA^a

| Entry | Catalyst | Pentan-2-one conversion / % | Selectivity / % | |
|-------|----------|-----------------------------|-----------------|-----------|
| | | | 1a | 1b |
| 1 | Pt/C | 91 | 2 | 98 |
| 2 | Ni/C | 58 | 97 | 3 |

^aReaction conditions: pentan-2-one (10 mmol), BA (10 mmol), Pt/C (0.002 g, 5 wt % Pt) or Ni/C (0.01 g, 10 wt % Ni), THF as a solvent (4.0 mL), 3.0 MPa H₂, 130 °C, and 1 h.

The corresponding values are listed in Table S5. As displayed in Figure 5A, B and D, the C=N bond distance of **1a** remained almost unchanged before and after adsorption on the Ni(111) surface, while the bond distance increased from 1.294 to 1.343 Å on the Pt(111) surface, suggesting **1a** can be activated on Pt(111). Meanwhile, as labeled in Figure 5C and E, the adsorption distance of **1a** on the Pt(111) surface was shorter than that on the Ni(111) surface, suggesting **1a** has a stronger affinity to the Pt surface. To further prove this, we calculated the adsorption energies of **1a** on both Pt(111) and Ni(111) surfaces. As expected, the former (-1.84 eV) was much higher than the latter (-0.21 eV). Moreover, the charge of the N atom changed from -0.4 to -0.36 e after **1a** was adsorbed on the Pt(111) surface, while the charge remained unchanged on Ni (Table S5), demonstrating a considerable charge transfer between **1a** and Pt. The electron transfer would promote the favorable chemisorption of **1a** on the Pt surface.⁶¹ In the literature, the reported H₂ chemisorption energies on Ni(111) and Pt(111) surfaces were -2.9⁶² and -0.77⁶³ eV, respectively, demonstrating H₂ has a stronger affinity to a Ni surface.

The Sabatier principle states that too weak or too strong of an interaction between a catalyst surface and adsorbed species will result in poor catalytic activity.⁶⁴ Apparently, for the Ni catalyst, the weak chemisorption of imines results in difficult activation, and the strong adsorption of H₂ molecules causes competitive adsorption of H₂, resulting in excessive blocking of the Ni surface sites, both of which eventually lead to poor hydrogenation activity. On the contrary, the Pt surfaces

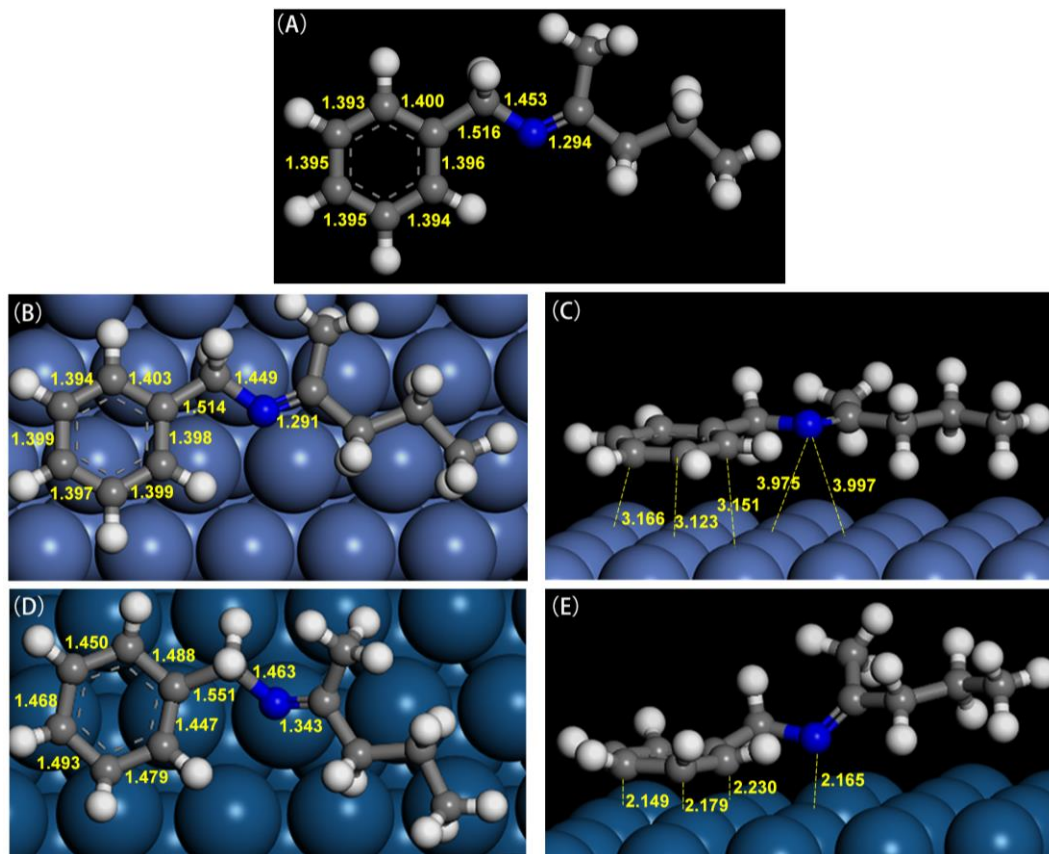


Figure 5. (A) Species **1a** before adsorption, and the top and side views of the adsorption of **1a** on (B, C) Ni(111) and (D, E) Pt(111) surfaces. Nickel atoms (●), platinum atoms (●), carbon atoms (●), oxygen atoms (●), and nitrogen atoms (●).

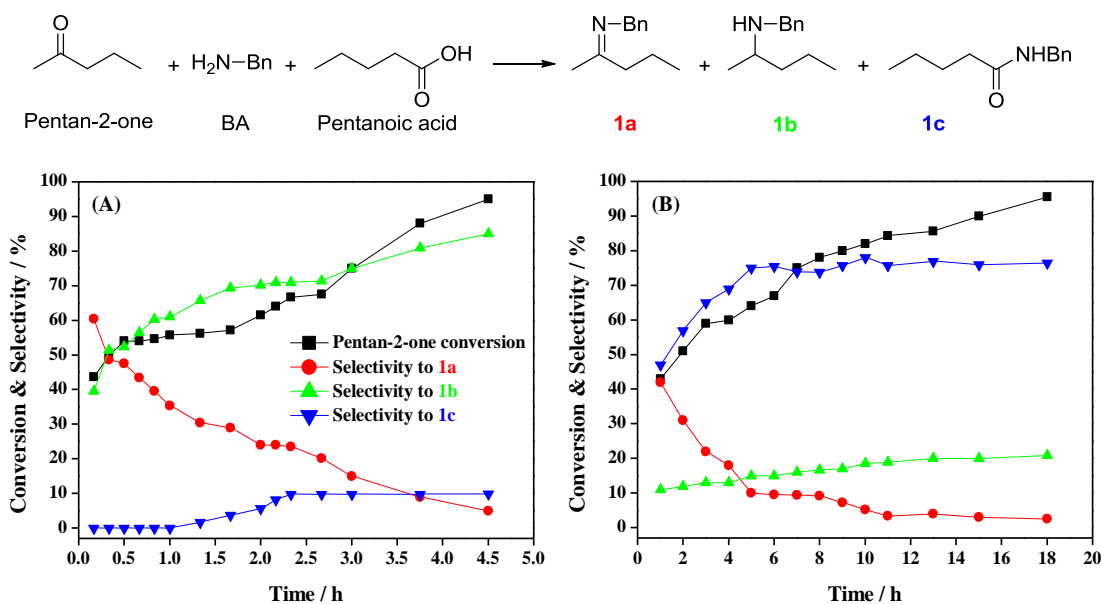


Figure 6. Effect of pentanoic acid on the reductive amination of pentan-2-one with BA over the (A) Pt/C and (B) Ni/C catalysts. Reaction conditions: pentan-2-one (10 mmol), BA (10 mmol), pentanoic acid (10 mmol), Pt/C (0.002 g, 5 wt % Pt) or Ni/C (0.01 g, 10 wt % Ni), THF as a solvent (4.0 mL), 3.0 MPa H_2 , and 130 °C.

showed relatively weak H_2 adsorption and high affinity to **1a**. These adsorption characteristics allow **1a** to be easily activated and subsequently hydrogenated by H_2 , providing high C=N hydrogenation activity over Pt/C.

We then attempted to examine if the difference in hydrogenation capability influenced the product distributions in the reductive amination reactions over the Pt/C and Ni/C catalysts.

Here, we used pentan-2-one to react with BA as an example. As expected, as shown in Table 3, we obtained 91% conversion of pentan-2-one with 98% selectivity to **1b** over Pt/C due to the high C=N hydrogenation activity. However, Ni/C provided imine **1a** as a major product with a poor pentan-2-one conversion (58%). The experimental results indicate that the large differences in C=N hydrogenation activity between Pt/C

and Ni/C effectively altered the product distributions in the reductive amination reactions.

To study the effect of the terminal carboxylic acid group in LA on the entire reaction, we introduced pentanoic acid as a mimic into the above reductive amination of pentan-2-one with BA. As shown in Figure 6, N-benzylpentanamide (**1c**) was generated through the condensation of BA and pentanoic acid, which will compete with the formation of **1a** from BA and pentan-2-one. For the Pt/C catalyst (Figure 6A), the hydrogenated product **1b** was primarily formed; **1c** was not found at the initial stages and only appeared with low selectivity (<10%) after 1.3 h. In contrast, for the Ni/C catalyst, the selectivity to **1c** gradually increased from 47 to 77%, while the selectivity to **1a** decreased from 42 to 2% with increased time (Figure 6B), indicating the hydrolysis of **1a** back to pentan-2-one and BA. Consequently, BA reacted with pentanoic acid to give **1c** as the major product. Based on the above analyses, we conclude that the large difference in the C=N hydrogenation activity between Pt/C and Ni/C switched the selectivity for the formation of imines/amides for the present reductive amination reaction. Therefore, regarding the reductive amination of LA with BA, we propose that Pt/C would favor the formation of imines as the first intermediate, which can then be efficiently hydrogenated to the corresponding amines, followed by cyclized dehydration to pyrrolidones (Scheme 1B). In contrast, Ni/C would promote the generation of amides as the first intermediate, which undergoes tandem cyclization, intramolecular dehydration and hydrogenation to give the final pyrrolidone (Scheme 1A).

Finally, we studied the application scope of the Ni-catalyzed reductive amination of LA with alkyl amines. As listed in Table S6, the reactions with alkyl amines (entries 1-4) and cycloalkyl amines (entries 5 and 6) completely converted LA with good yields (>84%) to the corresponding pyrrolidones after 10 h reactions. Note that the yields of the pyrrolidones strongly depended on the carbon chain length, which may be ascribed to the steric hindrance for the hydrogenation of 1-R-5-methylenepyrrolidin-2-one to pyrrolidones.

3. CONCLUSIONS

We successfully developed a facile ALD preparation of $\text{CNF}_x\text{@Ni@CNTs}$ catalysts with a thickness-controlled porous carbon coating on Ni NPs for the reductive amination of LA with amines to pyrrolidones under liquid-phase conditions. Under the protection of porous carbon with moderate thickness, the $\text{CNF}_{30}\text{@Ni@CNTs}$ catalyst was recycled for 20 runs without observable leaching or sintering of the Ni NPs. The porous and defective nature of the carbon shells with an appropriate thickness allowed reactants to easily access the underlying Ni NPs. On the other hand, we found the Ni-catalyzed reaction mechanism to be quite different from the previously reported noble-metal-catalyzed reaction pathway via imine intermediates. In our system, amides were first formed as the important intermediate and subsequently underwent tandem cyclization, intramolecular dehydration and hydrogenation to the desired pyrrolidones. C=N hydrogenation experiments and DFT calculations indicated that the weak adsorption of imines on the Ni surface had an adverse effect on the hydrogenation of imines. We also found that imines can be hydrolyzed back to LA and amines in the presence of carboxyl groups, which can competitively react with amines to afford amides. These findings provide an elaborate concept to design stable heterogeneous catalysts for use under liquid-phase conditions and to realize replacements for noble-metal catalysts for the conversion of multifunctional substrates.

4. EXPERIMENTAL SECTION

Preparation of the Catalysts. The $\text{CNF}_x\text{@Ni@CNTs}$ catalyst (10 wt % Ni) was fabricated by ALD. The deposition of NiO and PI were performed in a hot-wall, closed chamber-type ALD reactor. First, NiO NPs were deposited on CNTs using 200 ALD cycles at 300 °C with nickelocene and ozone as precursors. The former source was maintained at 75 °C. Then, NiO@CNTs was further coated by a PI film with x ($x = 0, 10, 20, 30, 50,$ and 80) cycles at 170 °C with ethylenediamine and pyromellitic dianhydride as precursors, which were maintained at 180 °C and room temperature, respectively. The as-prepared samples were treated under H_2/N_2 (10/90) at 600 °C for 2 h ($3\text{ }^\circ\text{C min}^{-1}$) to obtain $\text{CNF}_x\text{@Ni@CNTs}$.

The supported Ni catalysts (10 wt % Ni) were prepared by incipient wetness impregnation using an aqueous solution of $\text{Ni}(\text{NO}_3)_2 \cdot 6\text{H}_2\text{O}$ and various supports (SAPO-34, HZSM-5, NbOPO_4 , TiO_2 , C and CNTs). The as-prepared samples were reduced under H_2/N_2 (10/90) at 450 °C for 4 h and were denoted as Ni/support. The Pt/C catalyst (5 wt % Pt) was synthesized with the same procedure using H_2PtCl_6 as a precursor and with reduction at 250 °C for 2 h.

Catalyst Characterization. TEM measurements were performed on an FEI Tecnai G2 F20 S-Twin electron microscope operated at an acceleration voltage of 200 kV. The metal leaching was measured by ICP-AES using a Perkin-Elmer OPTIMA 3300 DV spectrometer (Norwalk, CT, U.S.A.). N_2 adsorption/desorption was performed using a Micromeritics ASAP 2020 instrument. Before the measurements, each sample was outgassed at 300 °C for 4 h under vacuum to remove moisture and volatile impurities.

Catalytic Reactions. The catalytic reactions were performed in a 100-mL stainless steel batch autoclave reactor (Parr Instrument Company). In a typical reaction, the reactor was loaded with LA (10 mmol), an amine (10 mmol), solvent (4 mL) and catalyst (0.03 g). The reactor was purged with H_2 five times then charged with 3 MPa H_2 and heated to 130 °C. After the reaction, the reactor was cooled to room temperature, and H_2 was released. Qualitative identification of the products was achieved by gas chromatography MS (GC-MS) (Agilent 5975C/7890A). The products **BMP**, **M3** and **M4** were quantified with 1,4-dioxane as an internal standard using a gas chromatograph (Agilent GC-7890A) equipped with an ATSE-54 capillary column ($60\text{ m} \times 0.32\text{ mm} \times 0.1\text{ }\mu\text{m}$) and a flame ionization detector. The quantitative analyses of **M1** and **M2** (external standard method) were performed using a high-performance liquid chromatography (Agilent 1260) apparatus equipped with an evaporative light scattering detector (ALLTECH 3300) and an Agilent 5 HC C18 (2) column ($250 \times 4.6\text{ mm}$).

General Procedure for the Recycling Test. After 4 h of reaction, the reactor was cooled, depressurized, and opened. Samples of the supernatant were taken for analysis. The catalyst was centrifuged, washed three times with γ -valerolactone and reused for the next run.

ASSOCIATED CONTENT

Supporting Information.

Chemicals and materials, computational details, N_2 physisorption isotherms, NH_3 -TPD, TEM, additional data of the catalytic experiments, and NMR, IR and HRMS characterization data of the products. This material is available free of charge via the Internet at <http://pubs.acs.org>.

AUTHOR INFORMATION

Corresponding Author

* E-mail for F.-W. Li: fuweili@licp.cas.cn

* E-mail for Y. Qin: qinyong@sxicc.ac.cn

ORCID

Fuwei Li: 0000-0003-2895-1185

Yong Qin: 0000-0002-5567-1464

Author Contributions

[§]These authors contributed equally.

Notes

The authors declare no competing financial interest.

ACKNOWLEDGMENT

This work was funded by the Natural Science Foundation of China (21503242, 21522309, 21633013 and 21673269), the Suzhou Science and Technology Projects (SYG201518 and SYG201519), the Chinese Academy of Sciences. The authors acknowledge Dr. Wei Lin from Northwestern University for computational discussions.

REFERENCES

- (1) Alonso, D. M.; Wettstein, S. G.; Dumesic, J. A. *Chem. Soc. Rev.* **2012**, *41*, 8075-8098.
- (2) Liu, B.; Zhang, Z. H. *ACS Catal.* **2016**, *6*, 326-338.
- (3) Li, C.; Zhao, X.; Wang, A.; Huber, G. W.; Zhang, T. *Chem. Rev.* **2015**, *115*, 11559-11624.
- (4) Geboers, J. A.; Van de Vyver, S.; Ooms, R.; Op de Beeck, B.; Jacobs, P. A.; Sels, B. F. *Catal. Sci. Tech.* **2011**, *1*, 714-726.
- (5) Ma, X. L.; Ma, R.; Hao, W. Y.; Chen, M. M.; Yan, F.; Cui, K.; Tian, Y.; Li, Y. D. *ACS Catal.* **2015**, *5*, 4803-4813.
- (6) Besson, M.; Gallezot, P.; Pinel, C. *Chem. Rev.* **2014**, *114*, 1827-1870.
- (7) Luska, K. L.; Migowski, P.; Leitner, W. *Green Chem.* **2015**, *17*, 3195-3206.
- (8) Ennaert, T.; Van Aelst, J.; Dijkmans, J.; De Clercq, R.; Schutyser, W.; Dusselier, M.; Verboekend, D.; Sels, B. F. *Chem. Soc. Rev.* **2016**, *45*, 584-611.
- (9) Guo, Z.; Liu, B.; Zhang, Q. H.; Deng, W. P.; Wang, Y.; Yang, Y. H. *Chem. Soc. Rev.* **2014**, *43*, 3480-3524.
- (10) Resasco, D. E.; Wang, B.; Crossley, S. *Catal. Sci. Technol.* **2016**, *6*, 2543-2559.
- (11) Liu, S. B.; Amada, Y.; Tamura, M.; Nakagawa, Y.; Tomishige, K. *Green Chem.* **2014**, *16*, 617-626.
- (12) Ma, R. F.; Wu, X. P.; Tong, T.; Shao, Z. J.; Wang, Y. Q.; Liu, X. H.; Xia, Q. N.; Gong, X. Q. *ACS Catal.* **2017**, *7*, 333-337.
- (13) Pan, T.; Deng, J.; Xu, Q.; Xu, Y.; Guo, Q. X.; Fu, Y. *Green Chem.* **2013**, *15*, 2967-2974.
- (14) Deng, T. Y.; Liu, H. C. *Green Chem.* **2013**, *15*, 116-124.
- (15) Sun, J. Y.; Liu, H. C. *Green Chem.* **2011**, *13*, 135-142.
- (16) Liu, Y.; Luo, C.; Liu, H. C. *Angew. Chem., Int. Ed.* **2012**, *51*, 3249-3253.
- (17) Xia, Q. N.; Xia, Y. J.; Xi, J. X.; Liu, X. H.; Zhang, Y. G.; Guo, Y.; Wang, Y. Q. *ChemSusChem* **2017**, *10*, 747-753.
- (18) Sádaba, I.; López Granados, M.; Riisager, A.; Taarning, E. *Green Chem.* **2015**, *17*, 4133-4145.
- (19) Lange, J. P. *Angew. Chem., Int. Ed.* **2015**, *54*, 13186-13197.
- (20) O'Neill, B. J.; Jackson, D. H.; Crisci, A. J.; Farberow, C. A.; Shi, F.; Alba-Rubio, A. C.; Lu, J.; Dietrich, P. J.; Gu, X.; Marshall, C. L.; Stair, P. C.; Elam, J. W.; Miller, J. T.; Ribeiro, F. H.; Voyles, P. M.; Greeley, J.; Mavrikakis, M.; Scott, S. L.; Kuech, T. F.; Dumesic, J. A. *Angew. Chem., Int. Ed.* **2013**, *52*, 13808-13812.
- (21) Gao, L. J.; Fu, Q.; Wei, M. M.; Zhu, Y. F.; Liu, Q.; Crumlin, E.; Liu, Z.; Bao, X. H. *ACS Catal.* **2016**, *6*, 6814-6822.
- (22) Deng, D. H.; Yu, L.; Chen, X. Q.; Wang, G. X.; Jin, L.; Pan, X. L.; Deng, J.; Sun, G. Q.; Bao, X. H. *Angew. Chem., Int. Ed.* **2013**, *52*, 371-375.
- (23) Lee, J.; Jackson, D. H. K.; Li, T.; Winans, R. E.; Dumesic, J. A.; Kuech, T. F.; Huber, G. W. *Energy Environ. Sci.* **2014**, *7*, 1657-1660.
- (24) Choi, M.; Wu, Z. J.; Iglesia, E. *J. Am. Chem. Soc.* **2010**, *132*, 9129-9137.
- (25) Liu, J. Y.; Chen, J. F.; Zhang, Y. *Catal. Sci. Tech.* **2013**, *3*, 2559-2564.
- (26) Goel, S.; Zones, S. I.; Iglesia, E. *J. Am. Chem. Soc.* **2014**, *136*, 15280-15290.
- (27) Wu, Z. J.; Goel, S.; Choi, M.; Iglesia, E. *J. Catal.* **2014**, *311*, 458-468.
- (28) Wang, N.; Sun, Q. M.; Bai, R. S.; Li, X.; Guo, G. Q.; Yu, J. H. *J. Am. Chem. Soc.* **2016**, *138*, 7484-7487.
- (29) Farrusseng, D.; Tuel, A. *New J. Chem.* **2015**, *40*, 3933-3949.
- (30) Wang, C. T.; Wang, L.; Zhang, J.; Wang, H.; Lewis, J. P.; Xiao, F. S. *J. Am. Chem. Soc.* **2016**, *138*, 7880-7883.
- (31) Zhan, B. Z.; Iglesia, E. *Angew. Chem., Int. Ed.* **2007**, *46*, 3697-3700.
- (32) Dasgupta, N. P.; Liu, C.; Andrews, S.; Prinz, F. B.; Yang, P. D. *J. Am. Chem. Soc.* **2013**, *135*, 12932-12935.
- (33) O'Neill, B. J.; Jackson, D. H. K.; Lee, J.; Canlas, C.; Stair, P. C.; Marshall, C. L.; Elam, J. W.; Kuech, T. F.; Dumesic, J. A.; Huber, G. W. *ACS Catal.* **2015**, *5*, 1804-1825.
- (34) Zhao, J. J.; Nunn, W. T.; Lemaire, P. C.; Lin, Y. L.; Dickey, M. D.; Oldham, C. J.; Walls, H. J.; Peterson, G. W.; Losego, M. D.; Parsons, G. N. *J. Am. Chem. Soc.* **2015**, *137*, 13756-13759.
- (35) Lu, J. L.; Liu, B.; Greeley, J. P.; Feng, Z. X.; Libera, J. A.; Lei, Y.; Bedzyk, M. J.; Stair, P. C.; Elam, J. W. *Chem. Mater.* **2012**, *24*, 2047-2055.
- (36) Li, X.; Lushington, A.; Sun, Q.; Xiao, W.; Liu, J.; Wang, B. Q.; Ye, Y. F.; Nie, K. Q.; Hu, Y. F.; Xiao, Q. F.; Li, R. Y.; Guo, J. H.; Sham, T. K.; Sun, X. L. *Nano. Lett.* **2016**, *16*, 3545-3549.
- (37) Lu, J. L.; Elam, J. W.; Stair, P. C. *Acc. Chem. Res.* **2013**, *46*, 1806-1815.
- (38) Lei, Y.; Lu, J.; Luo, X. Y.; Wu, T. P.; Du, P.; Zhang, X. Y.; Ren, Y.; Wen, J. G.; Miller, D. J.; Miller, J. T.; Sun, Y. K.; Elam, J. W.; Amine, K. *Nano. Lett.* **2013**, *13*, 4182-4189.
- (39) Lei, Y.; Liu, B.; Lu, J. L.; Lobo-Lapidus, R. J.; Wu, T. P.; Feng, H.; Xia, X. X.; Mane, A. U.; Libera, J. A.; Greeley, J. P.; Miller, J. T.; Elam, J. W. *Chem. Mater.* **2012**, *24*, 3525-3533.
- (40) Li, H.; Shao, Y. D.; Su, Y. T.; Gao, Y. H.; Wang, X. W. *Chem. Mater.* **2016**, *28*, 1155-1164.
- (41) Gao, Z.; Dong, M.; Wang, G. Z.; Sheng, P.; Wu, Z. W.; Yang, H. M.; Zhang, B.; Wang, G. F.; Wang, J. G.; Qin, Y. *Angew. Chem., Int. Ed.* **2015**, *54*, 9006-9010.
- (42) Wang, M. H.; Gao, Z.; Zhang, B.; Yang, H. M.; Qiao, Y.; Chen, S.; Ge, H. B.; Zhang, J. K.; Qin, Y. *Chem. - Eur. J.* **2016**, *22*, 8438-8443.
- (43) Yu, L.; Du, X. L.; Yuan, J.; Liu, Y. M.; Cao, Y.; He, H. Y.; Fan, K. N. *ChemSusChem* **2013**, *6*, 42-46.
- (44) Wright, W. R.; Palkovits, R. *ChemSusChem* **2012**, *5*, 1657-1667.
- (45) Pileidis, F. D.; Titirici, M. M. *ChemSusChem* **2016**, *9*, 562-582.
- (46) Yan, K.; Jarvis, C.; Gu, J.; Yan, Y. *Renewable Sustainable Energy Rev.* **2015**, *51*, 986-997.
- (47) Ledoux, A.; Sandjong Kuigwa, L.; Framery, E.; Andrioletti, B. *Green Chem.* **2015**, *17*, 3251-3254.
- (48) Wei, Y. W.; Wang, C.; Jiang, X.; Xue, D.; Liu, Z. T.; Xiao, J. L. *Green Chem.* **2014**, *16*, 1093-1096.
- (49) Vidal, J. D.; Climent, M. J.; Concepcion, P.; Corma, A.; Iborra, S.; Sabater, M. J. *ACS Catal.* **2015**, *5*, 5812-5821.
- (50) Chieffi, G.; Braun, M.; Esposito, D. *ChemSusChem* **2015**, *8*, 3590-3594.
- (51) Touchy, A. S.; Hakim Siddiki, S. M. A.; Kon, K.; Shimizu, K. *ACS Catal.* **2014**, *4*, 3045-3050.
- (52) Wei, Y. W.; Wang, C.; Jiang, X.; Xue, D.; Li, J.; Xiao, J. L. *Chem. Commun.* **2013**, *49*, 5408-5410.
- (53) Du, X. L.; He, L.; Zhao, S.; Liu, Y. M.; Cao, Y.; He, H. Y.; Fan, K. N. *Angew. Chem., Int. Ed.* **2011**, *50*, 7815-7819.
- (54) Huang, Y. B.; Dai, J. J.; Deng, X. J.; Qu, Y. C.; Guo, Q. X.; Fu, Y. *ChemSusChem* **2011**, *4*, 1578-1581.
- (55) Ortiz-Cervantes, C.; Flores-Alamo, M.; García, J. J. *Tetrahedron Lett.* **2016**, *57*, 766-771.
- (56) Vidal, J. D.; Climent, M. J.; Corma, A.; Concepcion, D. P.; Iborra, S. *ChemSusChem* **2017**, *10*, 119-128.
- (57) Chen, Y.; Gao, Z.; Zhang, B.; Zhao, S. C.; Qin, Y. *J. Power Sources* **2016**, *315*, 254-260.
- (58) Yang, P.; Wang, G. Z.; Gao, Z.; Chen, H.; Wang, Y.; Qin, Y. *Materials* **2013**, *6*, 5602-5612.

- 1 (59) Li, L.; Wang, T. H.; Liu, Q. L.; Cao, Y. M.; Qiu, J. S. *Carbon*
2 **2012**, *50*, 5186-5195.
- 3 (60) Padwa, A.; Rashatasakhon, P.; Rose, M. *J. Org. Chem.* **2003**, *68*,
4 5139-5146.
- 5 (61) Tang, M. H.; Mao, S. J.; Li, M. M.; Wei, Z. Z.; Xu, F.; Li, H. F.;
6 Wang, Y. *ACS Catal.* **2015**, *5*, 3100-3107.
- 7 (62) Bhatia, B.; Sholl, D. S. *J. Chem. Phys.* **2005**, *122*, 204707.
- 8 (63) Papoian, G.; Nørskov, J. K.; Hoffmann, R. *J. Am. Chem. Soc.*
9 **2000**, *122*, 4129-4144.
- 10 (64) Ertl, G.; Knözinger, H.; Schüth, F.; Weitkamp, J. *Handbook of*
11 *Heterogeneous Catalysis*, 2 nd ed.; Wiley-VCH Verlag GmbH & Co.
12 KgaA: New York, 2008; Vol. 1, p 3.
- 13
- 14
- 15
- 16
- 17
- 18
- 19
- 20
- 21
- 22
- 23
- 24
- 25
- 26
- 27
- 28
- 29
- 30
- 31
- 32
- 33
- 34
- 35
- 36
- 37
- 38
- 39
- 40
- 41
- 42
- 43
- 44
- 45
- 46
- 47
- 48
- 49
- 50
- 51
- 52
- 53
- 54
- 55
- 56
- 57
- 58
- 59
- 60

